R2: Heuristic Bug-Based Any-angle Path-Planning using Lazy Searches

Yan Kai Lai, Prahlad Vadakkepat, Abdullah Al Mamun, Cheng Xiang, Tong Heng Lee

***Abstract*—R2 is a novel online any-angle path planner that uses heuristic bug-based or ray casting approaches to find optimal paths in 2D maps with non-convex, polygonal obstacles. R2 is competitive to traditional free-space planners, finding paths quickly if queries have direct line-of-sight. On large sparse maps with few obstacle contours, which are likely to occur in practice, R2 outperforms free-space planners, and can be much faster than state-of-the-art free-space expansion planner Anya. On maps with many contours, Anya performs faster than R2. R2 is built on RayScan, introducing lazy-searches and a source-pledge counter to find successors optimistically on contiguous contours. The novel approach bypasses most successors on jagged contours to reduce expensive line-of-sight checks, therefore requiring no pre-processing to be a competitive online any-angle planner.**

***Index Terms*—2D Path Planning, Euclidean Shortest Paths, Any angle, Bug algorithms, Ray casting**

I. Introduction

In mobile robot path planning, global planners find paths between the robot and a destination. Traditional methods like A* [1] and Dijkstra [2] constrain shortest-path solutions to eight directions. Realistic, near-optimal any-angle paths can be obtained after post-processing, increasing the overall search time [3] [4].

Online methods do not require post or pre-processing to find paths [5] [6], and are suitable for dynamic situations by re-planning paths on updated maps. Online any-angle planners find any-angle paths. Theta* uses line-of-sight (LOS) checks and is slow [3], while Lazy-Theta* improves on Theta* by delaying LOS checks until expansion takes place [4]. Anya searches without LOS checks by strategically ignoring vertices that are not convex corners [5]. Anya is the state-of-the-art for online, free-space expansion planners, which searches over the free-space to find any-angle paths.

Deep reinforcement learning methods learn optimal trajectories by integrating kinematic and dynamic constraints with static, high dimensional maps. Deep reinforcement learning methods are only suitable for finding trajectories around local obstacles and constraints, requiring global planners to find paths between points [7]. The methods can be effective global planners, but require entire maps to be re-learnt, which is similar to pre-processing.

Random sampling algorithms such as Probabilistic Road Maps (PRM) [8] and Rapidly-exploring Random Trees (RRT) [9] are more suitable than online any-angle planners for high-dimensional global path planning, as finding optimal solutions is NP-hard [10], and random sampling algorithms find complete, near-optimal solutions quickly [8], [9]. In two dimensions (2D), online any-angle planners are viable as they return optimal paths quickly.

Online any-angle planners have so far relied on free-space expansions, and strategies to speed up planning can be made by taking inspiration from vector-based navigation, such as bug algorithms. Bug algorithms move directly to an intended objective [11], [12] can be used to bypass unnecessary free cells and reduce LOS checks to improve search time. The Pledge algorithm [13] is a bug algorithm that navigates around non-convex obstacles using one turn counter, inspiring a novel counter in the proposed R2 algorithm. Bug algorithms are not suitable as global planners as they do not incorporate heuristic costs to find optimal paths.

The heuristic-bug class of any-angle path planning incorporates heuristic costs to bug-based expansions. The heuristic-bug class is nascent and includes two planners. The planners do not always find paths in complex obstacles. Ray Path Finder (RPF) is not always terminable, and can have exponentially slow searches [14]. RayScan relies on pre-processing the occupancy grid into a visibility graph, and does not always work on non-convex obstacles [6]. LOS checks for unnecessary turning points are required in RayScan, particularly on obstacles with jagged structures.

The proposed R2 planner improves RayScan by correctly finding paths around non-convex polygonal obstacles, and quickly searching jagged structures without pre-processing. R2 improves search time in jagged structures by optimistically identifying successors and lazily verifying LOS. R2 identifies successors in non-convex obstacles by using a novel source-pledge counter. The novelty allows R2 to find optimal paths in non-convex obstacles. Section II provides an overview and pseudocode of R2. Section III proves the correctness of the source-pledge counter in identifying turning points. Section IV proves the correctness of R2. Sections V and VI show the methodology of comparing with Anya and the results.

II. Overview

R2 is listed in Algorithms 1 to 4. The queries are run from RUN. The nomenclature is based on [14] and [6]. R2 is built on top of RayScan, accelerating searches by optimistically searching for turning points to reduce LOS checks. R2 works without pre-processing, and is an online planner like Anya

The authors are from Department of Electrical and Computer Engineering, National University of Singapore

Algorithm 1 R2 Root Recursive Functions

function RUN($\mathbf{z}_\zeta = (x_\zeta, y_\zeta)$, $\mathbf{z}_g = (x_g, y_g)$)
  Clear $\mathbf{\Psi}$, $\mathbf{L}_{\text{open}}$, $\mathbf{L}_{\text{closed}}$ to $\emptyset$
  START_SUCCESSORS($(\mathbf{z}_\zeta, 0, \text{EUC}(\mathbf{z}_\zeta, \mathbf{z}_g), \emptyset)$)
  while $\mathbf{L}_{\text{open}}$ is not empty **and** $\mathbf{\Psi}$ is empty **do**
    SUCCESSORS(polled cheapest node from $\mathbf{L}_{\text{open}}$)
  end while
  return $\mathbf{\Psi}$
end function
function START_SUCCESSORS($\mathbf{n}_s = (\mathbf{z}_s, c_s, c_t, \mathbf{z}_p)$)
  Clear $\mathbf{H}$ to $\emptyset$
  Cast from $\mathbf{z}_s$ to $\mathbf{z}_g$
  if cast reached $\mathbf{z}_g$ **then**
    $\mathbf{\Psi} \leftarrow (\mathbf{z}_g, \mathbf{z}_s)$
  else ▷ cast collides at $\mathbf{z}_c$
    SCAN(L, $\mathbf{z}_c$, $\mathbf{z}_g$, $\mathbf{n}_s$, $\emptyset$)
    SCAN(R, $\mathbf{z}_c$, $\mathbf{z}_g$, $\mathbf{n}_s$, $\emptyset$)
  end if
end function
function SUCCESSORS($\mathbf{n}_s = (\mathbf{z}_s, c_s, c_t, \mathbf{z}_p)$)
  Clear $\mathbf{H}$ to $\emptyset$
  if $\mathbf{z}_g$ is in F.S. of $\mathbf{z}_s$ w.r.t. $\mathbf{z}_p$ **then**
    Cast from $\mathbf{z}_s$ to $\mathbf{z}_g$
    if cast reached $\mathbf{z}_g$ **then**
      Fill $\mathbf{\Psi}$ by recursively finding parents
    else ▷ Collided at $\mathbf{z}_c$
      SCAN(L, $\mathbf{z}_c$, $\mathbf{z}_g$, $\mathbf{n}_s$, $\emptyset$)
      SCAN(R, $\mathbf{z}_c$, $\mathbf{z}_g$, $\mathbf{n}_s$, $\emptyset$)
    end if
  end if ▷ Cast along radii of F.S.
  Cast along left radius of F.S. of $\mathbf{z}_s$ w.r.t. $\mathbf{z}_p$
  if cast collides at $\mathbf{z}_c$ **then**
    SCAN(L, $\mathbf{z}_c$, $\mathbf{z}_g$, $\mathbf{n}_s$, $\emptyset$)
  end if
  Cast along right radius of F.S. of $\mathbf{z}_s$ w.r.t. $\mathbf{z}_p$
  if cast collides at $\mathbf{z}_c$ **then**
    SCAN(R, $\mathbf{z}_c$, $\mathbf{z}_g$, $\mathbf{n}_s$, $\emptyset$)
  end if
end function

Algorithm 2 Recursive Scan

function SCAN(d, $\mathbf{z}_c$, $\mathbf{z}_t$, $\mathbf{n}_s = (\mathbf{z}_s, c_s, c_t, \mathbf{z}_p)$, $\mathbf{\Gamma}_p$)
  $(\eta_t, \mathbf{\Gamma}, \mathbf{\Gamma}_p) \leftarrow$TRACER($d$, $\mathbf{z}_c$, $\mathbf{z}_t$, $\mathbf{z}_s$, $\mathbf{n}_s$, $\emptyset$, $\mathbf{\Gamma}_p$) ▷ Spawn lazy-searches to find candidates in $\mathbf{\Gamma}$ and prune parent candidates in $\mathbf{\Gamma}_p$
  while $\mathbf{\Gamma}$ is not empty **do**
    Pop $\mathbf{z}_\gamma$ from $\mathbf{\Gamma}$ and push it to $\mathbf{H}$
    Cast from $\mathbf{z}_s$ to $\mathbf{z}_\gamma$
    if cast reached $\mathbf{z}_\gamma$ **then**
      Add $\mathbf{z}_\gamma$ as successor of $\mathbf{n}_s$
      Discard other candidates by emptying $\mathbf{\Gamma}$
      Infinite-cast from $\mathbf{z}_\gamma$ in direction $\overrightarrow{\mathbf{z}_s\mathbf{z}_\gamma}$
      if infinite-cast collides at $\mathbf{z}_c$ **then**
        SCAN(d, $\mathbf{z}_c$, $\mathbf{z}_g$, $\mathbf{n}_s$, $\mathbf{\Gamma}_p$)
      end if
    else ▷ Collide before reaching $\mathbf{z}_\gamma$
      if $d = L$ **then** ▷ L child is major
        SCAN(L, $\mathbf{z}_c$, $\mathbf{z}_\gamma$, $\mathbf{n}_s$, $\mathbf{\Gamma}_p$)
        SCAN(R, $\mathbf{z}_c$, $\mathbf{z}_\gamma$, $\mathbf{n}_s$, $\mathbf{\Gamma}$)
      else ▷ R child is major
        SCAN(L, $\mathbf{z}_c$, $\mathbf{z}_\gamma$, $\mathbf{n}_s$, $\mathbf{\Gamma}$)
        SCAN(R, $\mathbf{z}_c$, $\mathbf{z}_\gamma$, $\mathbf{n}_s$, $\mathbf{\Gamma}_p$)
      end if
    end if
  end while
end function

Algorithm 3 Lazy-search Caster

function CASTER($\mathbf{z}_m$, $\mathbf{z}_t$, d, $\mathbf{n}_s$, $\mathbf{\Gamma}$, $\mathbf{\Gamma}_p$)
  Cast from $\mathbf{z}_m$ to $\mathbf{z}_t$
  if cast reached $\mathbf{z}_t$ **then return** $(\mathbf{\Gamma}, \mathbf{\Gamma}_p)$
  $(\eta_t, \mathbf{\Gamma}, \mathbf{\Gamma}_p) \leftarrow$ TRACER($\neg d$, $\mathbf{z}_c$, $\mathbf{z}_t$, $\mathbf{z}_m$, $\mathbf{n}_s$, $\mathbf{\Gamma}$, $\mathbf{\Gamma}_p$)
  if η_t **then return** $(\mathbf{\Gamma}, \mathbf{\Gamma}_p)$ ▷ Cand. in minor tracer
  $(\eta_t, \mathbf{\Gamma}, \mathbf{\Gamma}_p) \leftarrow$ TRACER(d, $\mathbf{z}_c$, $\mathbf{z}_t$, $\mathbf{z}_m$, $\mathbf{n}_s$, $\mathbf{\Gamma}$, $\mathbf{\Gamma}_p$)
  return $(\mathbf{\Gamma}, \mathbf{\Gamma}_p)$
end function

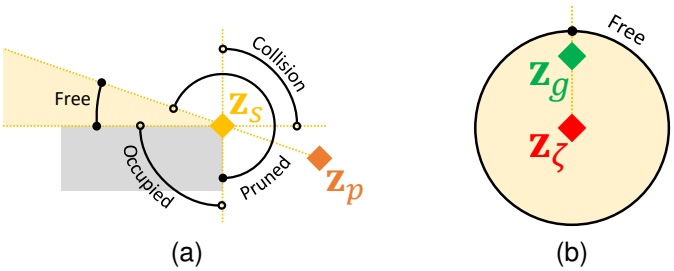

Fig. 1. (a) Sectors on convex corners. (b) Start $\mathbf{z}_\zeta$ only has the start sector, which is a circular free-sector

[5]. R2 is the first planner of the heuristic-bug class of any-angle planners [14] that finds optimal paths on maps with non-convex polygonal obstacles.

Path planners find paths between the **start** $\mathbf{z}_\zeta$ and **goal** $\mathbf{z}_g$. After polling from the **open list** $\mathbf{L}_{\text{open}}$, a **source** node $\mathbf{n}_s = (\mathbf{z}_s, c_s, c_t, \mathbf{z}_p)$, lying on either $\mathbf{z}_\zeta$ or convex corners, is expanded. Every node contains the cheapest g-cost c_s, h-cost c_t [1], coordinate of the cheapest parent $\mathbf{z}_p$ and the node's convex corner $\mathbf{z}_s$, that the planner knows so far.

In expanding the **source**, all relevant **successors**, or turning points with LOS to the source, are found. Every expansion uses **casts** and **traces**. Casts are straight-line collision checks, while traces follow obstacle contours. Traces can be **left** (L) or **right sided** (R), where the obstacle lies on the right and left of the trace respectively.

The **free-sector** (F.S., angular sector in RayScan) is a sector centered on $\mathbf{z}_s$ enclosed between two radii, both infinite in length. One of the radii is in the direction $\overrightarrow{\mathbf{z}_p\mathbf{z}_s}$, and the other is along the nearer obstacle edge adjacent to $\mathbf{z}_s$. The free-sector is **non-reflex**, where the **angle subtended** is $0 \leq \theta_{FS} < 180$, if $\mathbf{z}_s$ lies on a convex corner. The **start sector** is a free-sector, and is a full circle centered on $\mathbf{z}_s = \mathbf{z}_\zeta$. The radii point along $\overrightarrow{\mathbf{z}_\zeta\mathbf{z}_g}$ (whole angular sector in RayScan). The free-sector radii are examined in out-of-sector checks, and θ_{FS} includes both

Algorithm 4 lazy-search Tracer

function TRACER(d, $\mathbf{z}_c$, $\mathbf{z}_t$, $\mathbf{z}_o$, $\mathbf{n}_s = (\mathbf{z}_s, c_s, c_t, \mathbf{z}_p)$, $\mathbf{\Gamma}$, $\mathbf{\Gamma}_p$)
  $\mathbf{z}_q \leftarrow \mathbf{z}_p$
  Calculate $\theta_{p,0}$
  for $m = \{1, 2, \cdots\}$ **do**
    d-trace from $\mathbf{z}_{m-1}$ in $\hat{\theta}_{e,m}$ until out-of-map or $\mathbf{z}_m$
    if out-of-map **then return** $(\mathit{True}, \mathbf{\Gamma}, \mathbf{\Gamma}_p)$
    while $\mathbf{\Gamma}_p$ is not empty **do** ▷ Check parent cand.
      $\mathbf{z}_{p,\gamma} \leftarrow$ last element of $\mathbf{\Gamma}_p$
      if $\mathbf{z}_{p,\gamma}$ is occluded by trace **then**
        Pop $\mathbf{z}_{p,\gamma}$ from $\mathbf{\Gamma}_p$
      else if $\mathbf{z}_{p,\gamma}$ occludes trace **then**
        return (*False*, $\mathbf{\Gamma}$, $\mathbf{\Gamma}_p$)
      else if $\mathbf{z}_{p,\gamma}$ found by trace **then**
        return (*True*, $\mathbf{\Gamma}$, $\mathbf{\Gamma}_p$)
      else ▷ No occlusion
        break
      end if
    end while
    if $\mathbf{z}_m = \mathbf{z}_o$ or $\mathbf{z}_m = \mathbf{z}_t$ **then return** (*False*, $\mathbf{\Gamma}$, $\mathbf{\Gamma}_p$)

    Calculate $\theta_{p,m}$
    if $\mathbf{z}_m$ in O.S. of $\mathbf{z}_o$ **then**
      return (*True*, $\mathbf{\Gamma}$, $\mathbf{\Gamma}_p$)
    else if $\mathbf{z}_m$ not in F.S. of $\mathbf{z}_o$ wrt $\mathbf{z}_q$ **then**
      if $\mathbf{z}_o = \mathbf{z}_s$ **or** $\mathbf{z}_m$ not in F.S. of $\mathbf{z}_s$ wrt $\mathbf{z}_p$ **then**
        return (*False*, $\mathbf{\Gamma}$, $\mathbf{\Gamma}_p$)
      end if
      $(\mathbf{z}_o, \mathbf{z}_q) \leftarrow (\mathbf{z}_s, \mathbf{z}_p)$ ▷ out-of-sector only
      $\theta_{p,m} \leftarrow \left[\!\left[\mathrm{atan2}\left(\overrightarrow{\mathbf{z}_m\mathbf{z}_s}\right) - \mathrm{atan2}\left(\overrightarrow{\mathbf{z}_m\mathbf{z}_o}\right)\right]\!\right]$
    end if
    if New turning corner found s.t. $\mathbf{z}_m$ is convex **and**
        $\{[(d = L) \wedge (\theta_{p,m} > 0)] \vee$
        $[(d = R) \wedge (\theta_{p,m} < 0)]\}$ **then**
      if $\mathbf{z}_o \neq \mathbf{z}_s$ **then**
        return (*True*, $\mathbf{\Gamma}$, $\mathbf{\Gamma}_p$) ▷ 2 consecutive t.c.
      end if
      if $\mathbf{z}_m$ lies on radii of F.S. of $\mathbf{z}_s$ wrt $\mathbf{z}_p$ **then**
        return (*True*, $\mathbf{\Gamma}$, $\mathbf{\Gamma}_p$)
      else if $\mathbf{z}_m \in \mathbf{H}$ **then** ▷ Refound a candidate
        return (*False*, $\mathbf{\Gamma}$, $\mathbf{\Gamma}_p$) ▷ Do not repeat
      end if
      Push $\mathbf{z}_m$ into $\mathbf{\Gamma}$
      if $\mathbf{z}_t$ in F.S. of $\mathbf{z}_m$ wrt $\mathbf{z}_o$ **then**
        $(\mathbf{\Gamma}, \mathbf{\Gamma}_p) \leftarrow$ CASTER($\mathbf{z}_m$, $\mathbf{z}_t$, d, $\mathbf{n}_s$, $\mathbf{\Gamma}$, $\mathbf{\Gamma}_p$)
        return (*False*, $\mathbf{\Gamma}$, $\mathbf{\Gamma}_p$)
      end if
      Let $\hat{\theta}_{s,m+1} = \hat{\theta}_{e,m}$ in next iteration
      Let $\theta_{p,m+1} = \left[\!\left[\hat{\theta}_{s,m+1} - \hat{\theta}_{e,m+1}\right]\!\right]$ in next iter.
      $(\mathbf{z}_o, \mathbf{z}_q) \leftarrow (\mathbf{z}_s, \mathbf{z}_p)$
    end if
    $\mathbf{z}_m^- \leftarrow \mathbf{z}_m$
  end for
end function

radii. The **occupied-sector** (O.S.) is a sector centered on $\mathbf{z}_s$, and its radii lie along the obstacle edges adjacent to $\mathbf{z}_s$. The angle subtended does not include both radii.

The **source-pledge** is a counter inspired by the target-pledge [14] from Ray Path Finder [15] that identifies turning points in non-convex obstacles depending on the **winding** of the traces. With further checks, R2 correctly identifies all relevant successors in non-convex obstacles.

The functions START_SUCCESSORS, SUCCESSORS and SCAN are used, like RayScan. START_SUCCESSORS is SUCCESSORS for the start node. SUCCESSORS occurs for every poll of $\mathbf{z}_s$ from $\mathbf{L}_{\text{open}}$:

1) If $\mathbf{z}_g$ is in the free-sector of the $\mathbf{z}_s$, a cast is attempted. If it reaches $\mathbf{z}_g$, a **path** $\mathbf{\Psi}$ is found and R2 terminates. If it collides, L and R scans are generated from the collision.
2) If $\mathbf{z}_g$ is not in the free-sector, **infinite casts** are launched on both radii of the free-sector. When the infinite-cast on the L radius collides, an R scan is generated, and vice versa. Otherwise, nothing happens if the infinite-cast goes **out-of-map**.

SCAN begins by using a **lazy-search**, consisting of recursive traces (TRACER) and casts CASTER, to search for successor **candidates** $\mathbf{z}_\gamma$. Lazy-searches follow contiguous contours by terminating when two **consecutive** turning points are found by the source-pledge – the second lies in the free-sector of the first – or for other conditions in Lemma 2.3. All turning points found by the lazy-search are returned in a **candidate stack** $\mathbf{\Gamma}$, which is in a **clockwise** (CW) or **anti-clockwise** (AW) angular order when seen from $\mathbf{z}_s$.

For every **candidate** $\mathbf{z}_\gamma$ in the stack, SCAN tries to cast from $\mathbf{z}_s$ to it. If reached, all other candidates are ignored as the path must pass through $\mathbf{z}_\gamma$ on the contiguous contour. An infinite-cast continues from the reached $\mathbf{z}_\gamma$, invoking **child scans** when the infinite-cast collides with an obstacle. When $\mathbf{z}_\gamma$ is not reached, child scans are invoked at the collision to expand towards $\mathbf{z}_\gamma$, allowing exit points to be prioritised for faster searches. After returning from the child scans, SCAN repeatedly pops the stack until a candidate successor is reached.

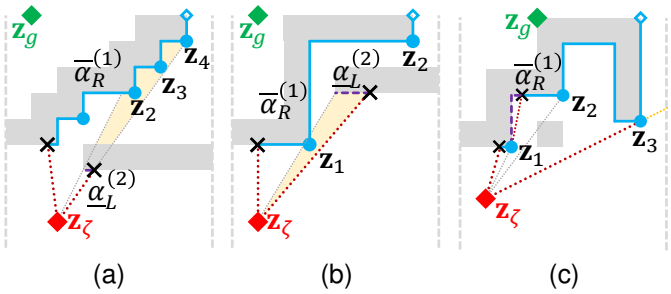

Fig. 2. Pruning parent candidates: (a) lazy-search in minor child scan $\underline{\alpha}_L^{(2)}$, invoked after cast to $\mathbf{z}_4$ collides in parent scan $\overline{\alpha}_R^{(1)}$, occludes and prunes parent candidates $\mathbf{z}_2$ and $\mathbf{z}_3$ from the parent stack $\mathbf{\Gamma}_{p,L}^{(2)} = \mathbf{\Gamma}_R^{(1)}$. (b) Parent candidate $\mathbf{z}_1$ occludes the lazy-search in the minor child scan $\underline{\alpha}_L^{(2)}$, terminating it. (c) All remaining candidates $\mathbf{z}_1$ and $\mathbf{z}_2$ in stack $\mathbf{\Gamma}^{(1)}$ are discarded as candidate $\mathbf{z}_3$ is reached, since they are part of the same contiguous contour.

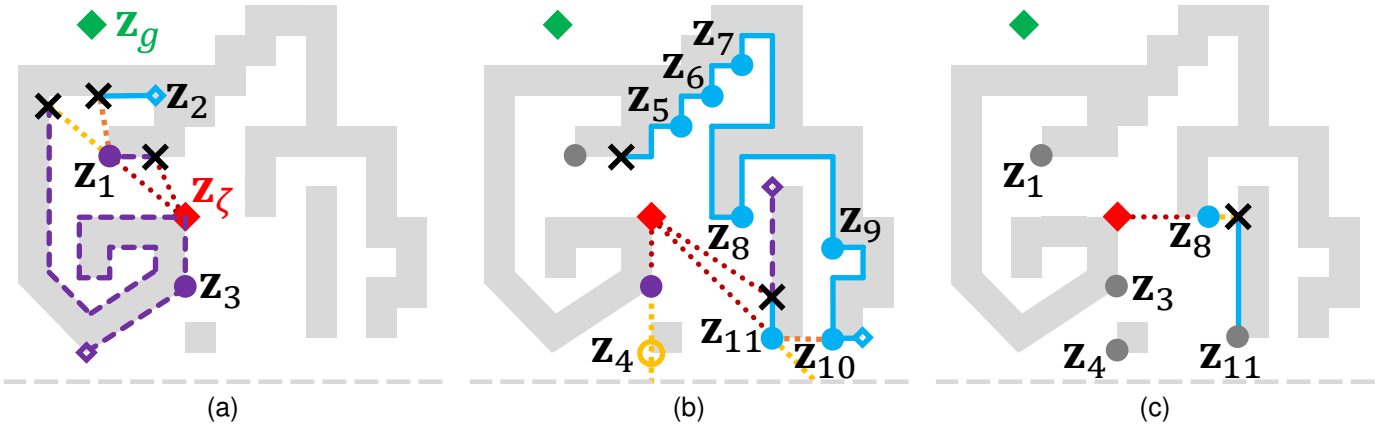

Fig. 3. Flow of R2 for START_SUCCESSORS. (a) After colliding when casting to $\mathbf{z}_g$, L-SCAN finds $\mathbf{z}_1$ in its lazy-search. The lazy-search optimistically casts (CASTER) to $\mathbf{z}_g$ as $\mathbf{z}_g$ is in the free-sector of $\mathbf{z}_1$ wrt $\mathbf{z}_\zeta$. CASTER collides, and the invoked minor TRACER enters the occupied-sector of $\mathbf{z}_1$, ending the lazy-search and returning $\mathbf{z}_1$ in the stack. SCAN casts and reaches $\mathbf{z}_1$, enqueuing it as a successor. The infinite-cast collides, invoking a child major SCAN, passing $\mathbf{z}_\zeta$ and finding $\mathbf{z}_3$ in a consecutive pair in the lazy-search. (b) The child SCAN casts to and enqueues successor $\mathbf{z}_3$, and $\mathbf{z}_4$ in an infinite-cast that goes out-of-map. Returning to START_SUCCESSORS, an R SCAN finds candidates $\mathbf{z}_5$ to $\mathbf{z}_{10}$ in its lazy-search, and collides while casting to candidate $\mathbf{z}_{10}$. The invoked L minor SCAN's lazy-search occludes $\mathbf{z}_9$, pruning $\mathbf{z}_9$ from the parent stack, and becomes obstructed by parent candidate $\mathbf{z}_8$, which returns control to the parent SCAN without candidates. An invoked R major SCAN finds $\mathbf{z}_{11}$ in its lazy-search, casting to and enqueuing $\mathbf{z}_{11}$ as a successor, and the infinite-cast goes out-of-map. (c) The child SCAN returns to the parent, casting to $\mathbf{z}_8$ and enqueueing $\mathbf{z}_8$ as a successor, discarding $\mathbf{z}_5$ to $\mathbf{z}_7$. An infinite-cast from $\mathbf{z}_8$ collides, finding $\mathbf{z}_{11} \in \mathbf{H}$ in an invoked SCAN, terminating all SCANs. START_SUCCESSORS ends, finding $\mathbf{z}_1$, $\mathbf{z}_3$, $\mathbf{z}_4$, $\mathbf{z}_8$ and $\mathbf{z}_{11}$ as successors.

Child scans are invoked when candidates on their parent scans are obstructed. A **major** and **minor** scan traces on the *same* and *opposite* sides (L or R) as the parent scan respectively. Every lazy-search checks against a **parent candidate stack** $\mathbf{\Gamma}_p$. A minor scan's parent stack is found by its parent scan, while a major scan's parent stack is inherited from the parent stack of its parent scan. The inheritance is correct as the contiguous contour followed by the child scan's lazy-search occurs between the child and parent scans' invoking casts, and the contour cannot intersect that parent scans' invoking casts. A minor scan may occlude and remove the parent candidates from the parent stack, while a major scan's lazy-search may occlude an ancestor scan if the latter's child is a minor scan. Lazy-searches are terminated if a parent candidate occludes them, or if the latter is re-discovered.

In a lazy-search, a **major** trace has the same sidedness (L or R) as the invoking scan, and a **minor** trace has the opposite sidedness. R2 prioritises minor traces with the terminability conditions in Lemma 2.3 to ensure that contiguous contours are followed in a lazy-search.

A **history** $\mathbf{H}$ of tested candidates is maintained for every call to SUCCESSORS (or START_SUCCESSORS). The SUCCESSORS' multiple calls to SCAN use the same history until it is cleared at the next call to SUCCESSORS for different $\mathbf{z}_s$. At every attempt to cast from $\mathbf{z}_s$ to $\mathbf{z}_\gamma$, the latter is pushed into $\mathbf{H}$. The lazy-search terminates if a turning point is in $\mathbf{H}$, as trace reversals after collided casts can re-generate repeated searches.

III. SOURCE-PLEDGE

A. Overview

The source-pledge monitors the winding of a compass that points away from an **origin** $\mathbf{z}_s$ along a trace. Turning points are identified when the source-pledge unwinds.

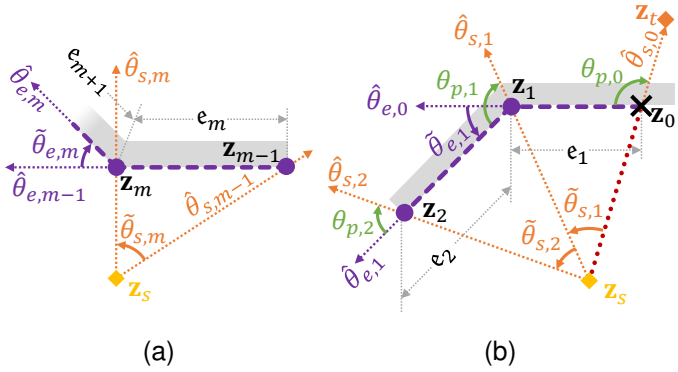

Fig. 4. Source-pledge notations (a) on edge $\mathfrak{e}_m$, and (b) near collision at $\mathbf{z}_0$.

Let, $[\![\theta]\!]^-$ be the angular restriction of θ such that $-\pi \leq \theta < \pi$. Let, $[\![\theta]\!]^+$ be the angular restriction of θ such that $-\pi < \theta \leq \pi$. Let, $[\![\cdot]\!]$ denote $[\![\cdot]\!]^+$ or $[\![\cdot]\!]^-$. For all $\theta_a \in \mathbb{R}$ and $\theta_b \in \mathbb{R}$:

Axiom 1. $[\![\theta_a - \theta_b]\!] = -[\![\theta_b - \theta_a]\!]$

Axiom 2. *If* $-\pi \leq \theta_a + \theta_b < \pi$ *then* $[\![\theta_a + \theta_b]\!] = \theta_a + \theta_b$

Axiom 3. $[\![\theta_a + \theta_b]\!] = [\![\theta_a - (2\pi k - \theta_b)]\!] \quad \forall \quad k \in \mathbb{Z}$

The source-pledge $\theta_{p,m}$ at the current corner $\mathbf{z}_m$ along the trace is:

$$\theta_{p,m} = \theta_{p,m-1} + \tilde{\theta}_{s,m} - \tilde{\theta}_{e,m}, \tag{1}$$

as shown in Fig. 4a. $\mathbf{z}_m$ occurs after tracing a straight edge $\mathfrak{e}_m$. $\tilde{\theta}_{s,m}$ is the angle at $\mathbf{z}_s$ subtended by $\mathfrak{e}_m$, and $\tilde{\theta}_{e,m}$ is the

change in trace headings:

$$[\![\theta]\!] = \begin{cases} [\![\theta]\!]^+ & \text{if left trace} \\ [\![\theta]\!]^- & \text{if right trace} \end{cases} \tag{2}$$

$$\tilde{\theta}_{s,m} = \left[\!\!\left[\hat{\theta}_{s,m} - \hat{\theta}_{s,m-1} \right]\!\!\right] \tag{3}$$

$$\tilde{\theta}_{e,m} = \left[\!\!\left[\hat{\theta}_{e,m} - \hat{\theta}_{e,m-1} \right]\!\!\right] \tag{4}$$

The range of $\tilde{\theta}_{s,m}$ depends on the limiting cases and side of the trace. Let the limiting case be such that $\mathbf{z}_s = \mathbf{z}_\zeta$ lie on the trace, so $\mathbf{z}_s$, $\mathbf{z}_m$ and $\mathbf{z}_{m-1}$ are colinear. An L trace yields $\tilde{\theta}_{s,m} = \pi$, and for a R trace $\tilde{\theta}_{s,m} = -\pi$. For $\tilde{\theta}_{e,m}$, when the trace stops at a corner, $-\pi < \tilde{\theta}_{e,m} < \pi$, and Eq. (4) can be either $[\![\cdot]\!]^+$ or $[\![\cdot]\!]^-$. $\tilde{\theta}_{s,m}$ and $\mathfrak{e}_m$ are **anticlockwise** (AW) or **clockwise** (CW) when viewed from $\mathbf{z}_s$.

$\hat{\theta}_{s,m}$ is the measured source heading and $\hat{\theta}_{e,m}$ is the measured heading of the next trace at $\mathbf{z}_m$:

$$\hat{\theta}_{s,m} = \operatorname{atan2}\left(\overrightarrow{\mathbf{z}_s\mathbf{z}_m}\right) \tag{5}$$

$$\hat{\theta}_{e,m} = \operatorname{atan2}\left(\overrightarrow{\mathbf{z}_m\mathbf{z}_{m+1}}\right) \tag{6}$$

where, $\hat{\theta}_{e,m}$ is known for polygons. $\mathbf{z}_0$ is the collision point, illustrated in Fig. 4b. At collision:

$$\hat{\theta}_{e,0} = \operatorname{atan2}\left(\overrightarrow{\mathbf{z}_0\mathbf{z}_1}\right) \tag{7}$$

$$\hat{\theta}_{s,0} = \operatorname{atan2}\left(\overrightarrow{\mathbf{z}_s\mathbf{z}_0}\right) \tag{8}$$

$$\hat{\theta}_{e,-1} = \hat{\theta}_{s,0} \tag{9}$$

$$\hat{\theta}_{s,-1} = \hat{\theta}_{s,0} \tag{10}$$

$$\theta_{p,-1} = 0 \tag{11}$$

in which the cast is a phantom trace where, the measured source and trace headings are identical. Let $\theta_{p,-1} = 0$:

$$\theta_{p,0} = -\left[\!\!\left[\hat{\theta}_{e,0} - \hat{\theta}_{s,0} \right]\!\!\right] = \left[\!\!\left[\hat{\theta}_{s,0} - \hat{\theta}_{e,0} \right]\!\!\right] \tag{12}$$

The angular range of $\theta_{p,0}$ is intuitive as casts can only collide on contours that are not parallel. The difference between the traced and source heading (casting direction for $m = 0$) is $-\pi < \theta_{p,0} < \pi$.

For all traces, $\theta_{p,m}$ is accumulated, lying in either one angular **half**, the **first or second quadrant** (Q1/Q2), or the **third or fourth quadrant** (Q3/Q4). Let, the edge $\mathfrak{e}_m$ be **exterior**, **interior**, or **occluded** when:

$$\text{Exterior } \mathfrak{e}_m := \begin{cases} -\pi \le \theta_{p,m-1} \le 0 & \text{if } L\text{-trace} \\ 0 \le \theta_{p,m-1} \le \pi & \text{if } R\text{-trace} \end{cases} \tag{13}$$

$$\text{Interior } \mathfrak{e}_m := \begin{cases} \theta_{p,m-1} < -\pi & \text{if } L\text{-trace} \\ \theta_{p,m-1} > \pi & \text{if } R\text{-trace} \end{cases} \tag{14}$$

$$\text{Occluded } \mathfrak{e}_m := \begin{cases} \theta_{p,m-1} > 0 & \text{if } L\text{-trace} \\ \theta_{p,m-1} < 0 & \text{if } R\text{-trace} \end{cases} \tag{15}$$

Fig. 5 and 6 show the general *L-trace* cases when $\theta_{p,m-1}$ lies in Q3/Q4, or Q1/Q2, respectively. Curved CW arrows in both figures depict positive angles, negative otherwise.

B. Edge Types

$\mathfrak{e}_m$ is distinguished based on the half $\theta_{p,m}$ lies in, allowing turning points to be identified:

Lemma 1.1. *All edges can be grouped into four types: (i) AW Q3/Q4 L-trace, (ii) CW Q1/Q2 L-trace, (iii) AW Q3/Q4 R-trace, (iv) CW Q3/Q4 R-trace.*

Proof. From Eq. (12), $\mathfrak{e}_1$ and $\theta_{p,0}$ must lie on Q3/Q4 for the L-trace and Q1/Q2 for the R-trace. The former is described in Table I and the latter in Table III. The edges, where $k = 0$, are exterior.

Table I shows the derivation for AW Q3/Q4 L-trace on $\mathfrak{e}_m$ which is illustrated in Fig. 5, with the conditions:

$$-2\pi(k + 0.5) \le \theta_{p,m-1} \le -2\pi k \quad \forall k \in \mathbb{Z} \tag{16}$$

$$0 \le \tilde{\theta}_{s,m} \le \pi. \tag{17}$$

When $|\mathfrak{e}_m| \to \infty$:

$$\tilde{\theta}_{s,m} < -\theta_{p,m-1} - 2\pi k \tag{18}$$

$$\theta_{p,m-1} + \tilde{\theta}_{s,m} < -2\pi k, \tag{19}$$

where, the RHS for Eq. (18) is less than π radians and positive, and rearranged into Eq. (19). Two-sided constraints for $\theta_{p,m-1} + \tilde{\theta}_{s,m}$ are obtained by adding Eq. (16) and (17):

$$-2\pi(k + 0.5) \le \theta_{p,m-1} + \tilde{\theta}_{s,m} \le -2\pi(k - 0.5), \tag{20}$$

and, intersected with Eq. (19) to obtain:

$$-2\pi(k + 0.5) \le \theta_{p,m-1} + \tilde{\theta}_{s,m} \le -2\pi k, \tag{21}$$

which is used for the cases 1 to 4 in Tables I, II, III and IV to derive the two-sided constraints for $\theta_{p,m}$.

For case 1, where $\mathfrak{e}_{m+1}$ is CW and $\mathbf{z}_m$ is convex:

$$-\pi < \tilde{\theta}_{s,m+1} < 0 \quad \iff \quad \hat{\theta}_{e,m} \times \hat{\theta}_{s,m} \tag{22}$$

$$-\pi < \tilde{\theta}_{e,m} < 0. \tag{23}$$

The initial constraints for $\theta_{p,m}$ in case 1 are obtained by subtracting Eq. (23) from (21):

$$-2\pi(k + 0.5) < \theta_{p,m} < -2\pi(k - 0.5). \tag{24}$$

Rewriting $\tilde{\theta}_{e,m}$ in terms of $\theta_{p,m-1}$ and $\tilde{\theta}_{s,m}$:

$$-\tilde{\theta}_{e,m} > -\theta_{p,m-1} - 2\pi k - \tilde{\theta}_{s,m} \tag{25}$$

$$\theta_{p,m} > -2\pi k, \tag{26}$$

where, Eq. (26) is rearranged from Eq. (25) using Eq. (1). The constraints for $\theta_{p,m}$ are obtained from the intersection of Eq. (24) and (26):

$$-2\pi k < \theta_{p,m} < -2\pi(k - 0.5), \tag{27}$$

which matches the constraint of $\theta_{p,m}$ for case 1 in Table I. All other cases can be derived in a similar manner, and found to lead to each other in Tables I, II, III and IV. □

From Tables I, II, III and IV, an unwound and wound pledge from the previous edge $\mathfrak{e}_{m+1}$ have smaller and larger k values than the current edge $\mathfrak{e}_m$.

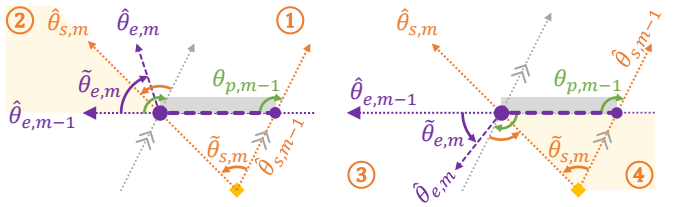

Fig. 5. Source-pledge cases for L trace, $0 \le \tilde{\theta}_{s,m} \le \pi$ and $-2\pi(k+0.5) < \theta_{p,m-1} \le -2\pi k$ (Q3/Q4). (a) $\mathbf{z}_m$ is convex. (b) $\mathbf{z}_m$ is non-convex.

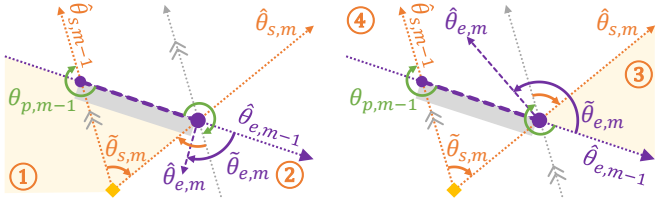

Fig. 6. Source-pledge cases for L trace, $-\pi < \tilde{\theta}_{s,m} \le 0$ and $-2\pi(k+1) < \theta_{p,m-1} \le -2\pi(k+0.5)$ (Q1/Q2). (a) $\mathbf{z}_m$ is convex. (b) $\mathbf{z}_m$ is non-convex.

TABLE I
AW Q3/Q4 L-TRACE ON $\mathfrak{e}_m$

Conditions for AW Q3/Q4 L-trace on $\mathfrak{e}_m$
Q3/Q4 $\theta_{p,m-1}$: $-2\pi(k+0.5) \le \theta_{p,m-1} \le -2\pi k \quad \forall k \in \mathbb{Z}$
AW $\mathfrak{e}_m$: $0 \le \tilde{\theta}_{s,m} \le \pi$
Case 1: CW $\mathfrak{e}_{m+1}$ around Convex $\mathbf{z}_m$
CW $\mathfrak{e}_{m+1}$: $-\pi < \tilde{\theta}_{s,m+1} < 0 \iff \hat{\theta}_{e,m} \times \hat{\theta}_{s,m} > 0$
Convex $\mathbf{z}_m$: $-\pi < \tilde{\theta}_{e,m} < 0$
Unwounded Q1/Q2 $\theta_{p,m}$: $-2\pi k < \theta_{p,m} < -2\pi(k-0.5)$
Case 2: AW $\mathfrak{e}_{m+1}$ around Convex $\mathbf{z}_m$
AW $\mathfrak{e}_{m+1}$: $0 \le \tilde{\theta}_{s,m+1} < \pi \iff \hat{\theta}_{e,m} \times \hat{\theta}_{s,m} \le 0$
Convex $\mathbf{z}_m$: $-\pi < \tilde{\theta}_{e,m} < 0$
Same Q3/Q4 $\theta_{p,m}$: $-2\pi(k+0.5) < \theta_{p,m} \le -2\pi k$
Case 3: AW $\mathfrak{e}_{m+1}$ around Non-convex $\mathbf{z}_m$
AW $\mathfrak{e}_{m+1}$: $0 \le \tilde{\theta}_{s,m+1} \le \pi \iff \hat{\theta}_{e,m} \times \hat{\theta}_{s,m} \le 0$
Non-convex $\mathbf{z}_m$: $0 < \tilde{\theta}_{e,m} < \pi$
Same Q3/Q4 $\theta_{p,m}$: $-2\pi(k+0.5) \le \theta_{p,m} < -2\pi k$
Case 4: CW $\mathfrak{e}_{m+1}$ around Non-convex $\mathbf{z}_m$
CW $\mathfrak{e}_{m+1}$: $-\pi < \tilde{\theta}_{s,m+1} < 0 \iff \hat{\theta}_{e,m} \times \hat{\theta}_{s,m} > 0$
Non-convex $\mathbf{z}_m$: $0 < \tilde{\theta}_{e,m} < \pi$
Wounded Q1/Q2 $\theta_{p,m}$: $-2\pi(k+1) < \theta_{p,m} < -2\pi(k+0.5)$

TABLE II
CW Q1/Q2 L-TRACE ON $\mathfrak{e}_m$

Conditions for CW Q1/Q2 L-trace on $\mathfrak{e}_m$
Q1/Q2 $\theta_{p,m-1}$: $-2\pi k < \theta_{p,m-1} < -2\pi(k-0.5) \quad \forall k \in \mathbb{Z}$
CW $\mathfrak{e}_m$: $-\pi < \tilde{\theta}_{s,m} < 0$
Case 1: AW $\mathfrak{e}_{m+1}$ around Convex $\mathbf{z}_m$
AW $\mathfrak{e}_{m+1}$: $-\pi \le \tilde{\theta}_{s,m+1} \le 0 \iff \hat{\theta}_{e,m} \times \hat{\theta}_{s,m} \le 0$
Convex $\mathbf{z}_m$: $-\pi < \tilde{\theta}_{e,m} < 0$
Unwounded Q3/Q4 $\theta_{p,m}$: $-2\pi(k-0.5) < \theta_{p,m} < -2\pi(k-1)$
Case 2: CW $\mathfrak{e}_{m+1}$ around Convex $\mathbf{z}_m$
CW $\mathfrak{e}_{m+1}$: $-\pi < \tilde{\theta}_{s,m+1} < 0 \iff \hat{\theta}_{e,m} \times \hat{\theta}_{s,m} > 0$
Convex $\mathbf{z}_m$: $-\pi < \tilde{\theta}_{e,m} < 0$
Same Q1/Q2 $\theta_{p,m}$: $-2\pi k < \theta_{p,m} < -2\pi(k-0.5)$
Case 3: CW $\mathfrak{e}_{m+1}$ around Non-convex $\mathbf{z}_m$
CW $\mathfrak{e}_{m+1}$: $-\pi < \tilde{\theta}_{s,m+1} < 0 \iff \hat{\theta}_{e,m} \times \hat{\theta}_{s,m} > 0$
Non-convex $\mathbf{z}_m$: $0 < \tilde{\theta}_{e,m} < \pi$
Same Q1/Q2 $\theta_{p,m}$: $-2\pi k \le \theta_{p,m} < -2\pi(k-0.5)$
Case 4: AW $\mathfrak{e}_{m+1}$ around Non-convex $\mathbf{z}_m$
AW $\mathfrak{e}_{m+1}$: $0 \le \tilde{\theta}_{s,m+1} < \pi \iff \hat{\theta}_{e,m} \times \hat{\theta}_{s,m} \le 0$
Non-convex $\mathbf{z}_m$: $0 < \tilde{\theta}_{e,m} < \pi$
Wounded Q3/Q4 $\theta_{p,m}$: $-2\pi(k+0.5) < \theta_{p,m} < -2\pi k$

TABLE III
CW Q1/Q2 R-TRACE ON $\mathfrak{e}_m$

Conditions for CW Q1/Q2 R-trace on $\mathfrak{e}_m$
Q1/Q2 $\theta_{p,m-1}$: $2\pi k \le \theta_{p,m-1} \le 2\pi(k+0.5) \quad \forall k \in \mathbb{Z}$
CW $\mathfrak{e}_m$: $-\pi \le \tilde{\theta}_{s,m} \le 0$
Case 1: AW $\mathfrak{e}_{m+1}$ around Convex $\mathbf{z}_m$
AW $\mathfrak{e}_{m+1}$: $0 < \tilde{\theta}_{s,m+1} < \pi \iff \hat{\theta}_{e,m} \times \hat{\theta}_{s,m} < 0$
Convex $\mathbf{z}_m$: $0 < \tilde{\theta}_{e,m} < \pi$
Unwounded Q3/Q4 $\theta_{p,m}$: $2\pi(k-0.5) < \theta_{p,m} < 2\pi k$
Case 2: CW $\mathfrak{e}_{m+1}$ around Convex $\mathbf{z}_m$
CW $\mathfrak{e}_{m+1}$: $-\pi < \tilde{\theta}_{s,m+1} \le 0 \iff \hat{\theta}_{e,m} \times \hat{\theta}_{s,m} \ge 0$
Convex $\mathbf{z}_m$: $0 < \tilde{\theta}_{e,m} < \pi$
Same Q1/Q2 $\theta_{p,m}$: $2\pi k \le \theta_{p,m} < 2\pi(k+0.5)$
Case 3: CW $\mathfrak{e}_{m+1}$ around Non-convex $\mathbf{z}_m$
CW $\mathfrak{e}_{m+1}$: $-\pi \le \tilde{\theta}_{s,m+1} \le 0 \iff \hat{\theta}_{e,m} \times \hat{\theta}_{s,m} \ge 0$
Non-convex $\mathbf{z}_m$: $-\pi < \tilde{\theta}_{e,m} < 0$
Same Q1/Q2 $\theta_{p,m}$: $2\pi k < \theta_{p,m} \le 2\pi(k+0.5)$
Case 4: AW $\mathfrak{e}_{m+1}$ around Non-convex $\mathbf{z}_m$
AW $\mathfrak{e}_{m+1}$: $0 < \tilde{\theta}_{s,m+1} < \pi \iff \hat{\theta}_{e,m} \times \hat{\theta}_{s,m} < 0$
Non-convex $\mathbf{z}_m$: $-\pi < \tilde{\theta}_{e,m} < 0$
Wounded Q3/Q4 $\theta_{p,m}$: $2\pi(k+0.5) < \theta_{p,m} < 2\pi(k+1)$

TABLE IV
AW Q3/Q4 R-TRACE ON $\mathfrak{e}_m$

Conditions for AW Q3/Q4 R-trace on $\mathfrak{e}_m$
Q3/Q4 $\theta_{p,m-1}$: $2\pi(k-0.5) < \theta_{p,m-1} < 2\pi k \quad \forall k \in \mathbb{Z}$
AW $\mathfrak{e}_m$: $0 < \tilde{\theta}_{s,m} < \pi$
Case 1: CW $\mathfrak{e}_{m+1}$ around Convex $\mathbf{z}_m$
CW $\mathfrak{e}_{m+1}$: $-\pi \le \tilde{\theta}_{s,m+1} \le 0 \iff \hat{\theta}_{e,m} \times \hat{\theta}_{s,m} \ge 0$
Convex $\mathbf{z}_m$: $0 < \tilde{\theta}_{e,m} < \pi$
Unwounded Q1/Q2 $\theta_{p,m}$: $2\pi(k-1) < \theta_{p,m} \le 2\pi(k-0.5)$
Case 2: AW $\mathfrak{e}_{m+1}$ around Convex $\mathbf{z}_m$
AW $\mathfrak{e}_{m+1}$: $0 < \tilde{\theta}_{s,m+1} < \pi \iff \hat{\theta}_{e,m} \times \hat{\theta}_{s,m} < 0$
Convex $\mathbf{z}_m$: $0 < \tilde{\theta}_{e,m} < \pi$
Same Q3/Q4 $\theta_{p,m}$: $2\pi(k-0.5) < \theta_{p,m} < 2\pi k$
Case 3: AW $\mathfrak{e}_{m+1}$ around Non-convex $\mathbf{z}_m$
AW $\mathfrak{e}_{m+1}$: $0 < \tilde{\theta}_{s,m+1} < \pi \iff \hat{\theta}_{e,m} \times \hat{\theta}_{s,m} < 0$
Non-convex $\mathbf{z}_m$: $-\pi < \tilde{\theta}_{e,m} < 0$
Same Q3/Q4 $\theta_{p,m}$: $2\pi(k-0.5) \le \theta_{p,m} < 2\pi k$
Case 4: CW $\mathfrak{e}_{m+1}$ around Non-convex $\mathbf{z}_m$
CW $\mathfrak{e}_{m+1}$: $-\pi < \tilde{\theta}_{s,m+1} \le 0 \iff \hat{\theta}_{e,m} \times \hat{\theta}_{s,m} \ge 0$
Non-convex $\mathbf{z}_m$: $-\pi < \tilde{\theta}_{e,m} < 0$
Wounded Q1/Q2 $\theta_{p,m}$: $2\pi k \le \theta_{p,m} < 2\pi(k+0.5)$

Corollary 1.1. *If $\tilde{\theta}_{s,m+1}$ is not in the same angular direction as $\tilde{\theta}_{s,m}$, then (i) $\theta_{p,m}$ is wound from $\theta_{p,m-1}$ if $\mathbf{z}_m$ is a non-convex corner, (ii) $\theta_{p,m}$ is unwound from $\theta_{p,m-1}$ if $\mathbf{z}_m$ is a convex corner.*

Condition (i) refers to case 1 in Tables I, II, III and IV, while condition (ii) refers to case 4.

Let the **winding** $h_w(\theta_{p,m}) = h_w(\mathbf{z}_m) = h_w(\mathfrak{e}_{m+1})$ be the wound half that $\theta_{p,m}$ belongs to, and let $h_w(\cdot) = 0$ for all exterior edges, so $h_w(\theta_{p,0}) = 0$. Interior edges have $h_w(\cdot) < 0$ and occluded edges have $h_w(\cdot) > 0$. The winding increases if $\theta_{p,m}$ is wound from $\theta_{p,m-1}$, decreases if it is unwound. Case 1 in Tables I, II, III and IV cause $h_w(\cdot)$ to decrement, and case 4 cause $h_w(\cdot)$ to increment.

C. General Topology

Turning points can be identified with Corollary 1.1, as turning points occur on corners where a trace passing through them changes the angular direction with respect to $\mathbf{z}_s$ [6]. Any map can be topologically redefined for every $\mathbf{z}_s$ where only the **turning corners** in Corollary 1.1 exist.

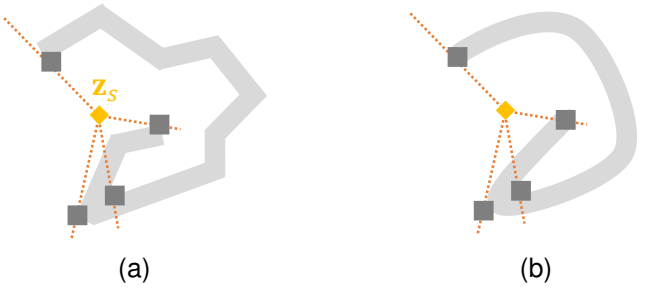

Fig. 7. Only turning corners are important in source-pledge. (a) Adjacent edges lying on the same angular half (b) can be re-defined as a topological curve.

Let a contiguous ordered set of traced edges $(\mathfrak{e}_m, \mathfrak{e}_{m+1}, \cdots, \mathfrak{e}_{m+n})$ be such that only the corners $\mathbf{z}_{m-1}$ and $\mathbf{z}_{m+n}$ cause the trace to change **direction** (AW to CW, or in reverse). These edges are topologically identical to a traced curve with turning corners at $\mathbf{z}_{m-1}$ and $\mathbf{z}_{m+n}$, and where $\theta_{p,m-1}$ and $\theta_{p,m+n-1}$ lie in the same angular half (Q1/Q2 or Q3/Q4), as shown in Fig. 7.

Let a topological curve $\mathfrak{c}_a$ be bound by turning corners at $\mathbf{z}_a$ and $\mathbf{z}_b$, with pledge $\theta_{p,a}$. Let, an **extrusion** be formed between $\mathbf{z}_a$ and $\mathbf{z}_b$ using turning corners at $\mathbf{z}_{a+1}, \mathbf{z}_{a+2}, \cdots, \mathbf{z}_{a+A}$ such that $h_w(\mathbf{z}_{a+A}) = h_w(\mathbf{z}_a)$, and the extrusion does not intersect other curves or itself. Due to Corollary 1.1, the same number of convex and non-convex turning corners exist for the winding to be equal. Extrusion examples are shown in Fig. 8.

For all contiguous contours that can be traced after a cast from the source, three basic topological forms exist, as illustrated in Fig. 9. The non-enclosed form does not enclose the source, and have at least n more convex turning corners where $n \geq 2k \ni k \in \mathbb{Z}^+$. The enclosed form encloses $\mathbf{z}_s$, and has the same number of convex and non-convex turning corners. The third form has at most two edges intersecting the map boundary, causing traces to trace out-of-map. The

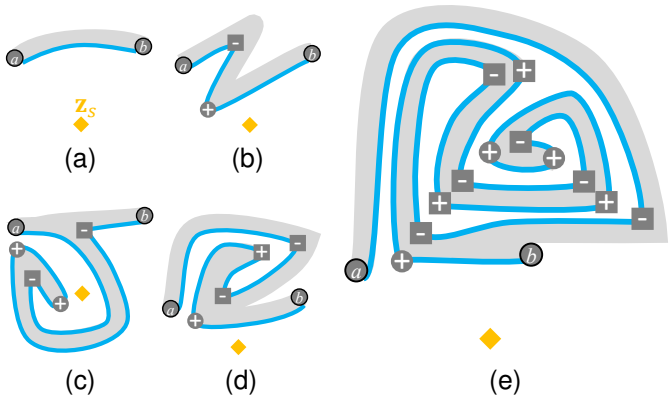

Fig. 8. Extrusion examples from non-enclosed topological form.

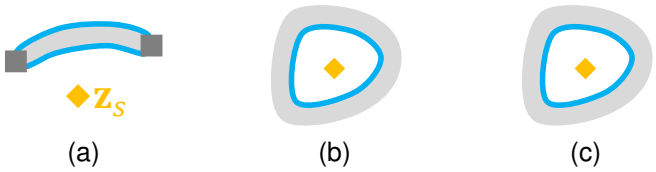

Fig. 9. Basic topologies: (a) Non-enclosed. (b) Enclosed. (c) Out-of-map.

three forms can be extended into arbitrary obstacles using extrusions. With the general topology:

Lemma 1.2. *Any convex turning corner $\mathbf{z}_m$ satisfying (i) $h_w(\theta_{p,m}) = -1$, (ii) $h_w(\theta_{p,m}) = 0$ or (iii) $h_w\theta_{p,m} < -1$, may have LOS from $\mathbf{z}_s$. All other convex turning corners satisfying (iv) $h_w(\theta_{p,m}) < 0$, do not have LOS.*

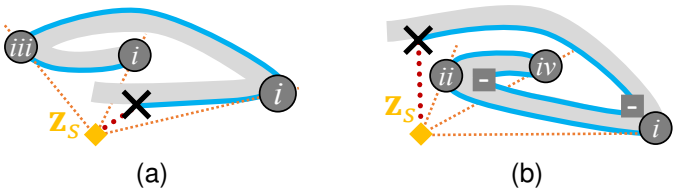

Fig. 10. Turning corners satisfying conditions (i) to (iv) in Lemma 1.2.

Proof. All convex turning corners are identified when $h_w(\theta_{p,m}) = h_w(\theta_{p,m-1}) - 1$. Let any topological curve be modified with extrusions. The convex turning corners identified between occluded edges, satisfying condition (iii), where $h_w(\theta_{p,m-1}) < 0$ may be visible from $\mathbf{z}_s$, if there are no obstructions. The obstructions can be other obstacles, or prior traced edges.

Turning corners satisfying conditions (i) and (ii) lie on the ends of a topological curve consisting of exterior edges. Exterior edges always face the source, and have LOS from $\mathbf{z}_s$, if there are no obstructions between the turning corners and $\mathbf{z}_s$.

Every convex turning corner identified between interior edges, where $h_w(\theta_{p,m-1}) > 1$ are not visible due to prior interior edges, as these corners can only occur after at least two non-convex turning corners.

□

Lemma 1.2 guarantees that turning corners in occluded and interior edges do not have LOS. The lemma does not guarantee LOS on turning corners satisfying conditions (i), (ii) or (iii). Examples of unobstructed convex turning corners satisfying conditions (i), (ii) or (iii) are shown as gray circles in Fig. 8b, 8c and 8d. Obstructed convex turning corners satisfying conditions (i), (ii) and (iii) can exist within nested spiral extrusions like the innermost corners in Fig. 8e.

D. Identifying Turning Points

Lemma 1.3. *A cast from $\mathbf{z}_s$ to $\mathbf{z}_t$ collides at $\mathbf{z}_0$. Let the first corner $\mathbf{z}_\gamma$ that satisfies condition (i) in Lemma 1.2 be found on the same trace after $\mathbf{z}_0$. Let a polygon P be bounded by $\overrightarrow{\mathbf{z}_s\mathbf{z}_0}$, $\overrightarrow{\mathbf{z}_s\mathbf{z}_\gamma}$, and edges traced between the corners $\mathbf{z}_0$ and $\mathbf{z}_\gamma$. If $\mathbf{z}_\gamma$ has LOS from $\mathbf{z}_s$, the shortest path that passes through $\mathbf{z}_s$ and $\mathbf{z}_t$ cannot intersect any corner within P.*

Proof. From Lemma 1.1, all edges between $\mathbf{z}_0$ and $\mathbf{z}_\gamma$ are either interior or exterior edges. No turning corners satisfying condition (iii) in Lemma 1.2 were found before $\mathbf{z}_\gamma$. Let $\mathbf{z}_n$ be a corner found before $\mathbf{z}_\gamma$ that satisfies condition (ii) in Lemma 1.2. If $\mathbf{z}_n$ lies on the shortest path, then $\theta_{p,n} = 0$ and $\mathbf{z}_n$ must lie between $\mathbf{z}_\gamma$ and $\mathbf{z}_s$ within the line $\overrightarrow{\mathbf{z}_s\mathbf{z}_\gamma}$. $\mathbf{z}_n$ can be ignored as $\mathbf{z}_s$ can reach $\mathbf{z}_\gamma$. When $\theta_{p,n} \neq 0$, the shortest path cannot pass through $\mathbf{z}_n$, as the path has to pass through the obstacles or detour. Turning corners satisfying condition (ii) can be ignored before finding $\mathbf{z}_\gamma$.

If $\mathbf{z}_\gamma$ does not have LOS from $\mathbf{z}_s$, and if $\mathbf{z}_\gamma$ is part of the shortest path, then a turning point can lie in P. If there is LOS, $\mathbf{z}_\gamma$ can lie along a shortest path solution from $\mathbf{z}_s$ to $\mathbf{z}_t$, as other corners in P will cause the path to detour. □

Corollary 1.2. *From Lemma 1.3, for the first turning corner $\mathbf{z}_\gamma$ that satisfies condition (i) of Lemma 1.2 along a trace, $\theta_{p,\gamma} > 0$ for an L-trace, or $\theta_{p,\gamma} < 0$ for an R-trace.*

Lemma 1.3 simplifies the cast and trace algorithms by stopping at turning corners satisfying condition (i). Turning corners satisfying condition (iii) can be found by Algorithm 5 by casting to turning corners satisfying condition (i). Algorithm 5 is built upon RayScan with Corollary 1.2, with a history check and no shrinking of free-sector.

Removing the shrinking of free-sector can repeat searches. $\mathbf{H}$ is a history of turning corners that were cast to in SCAN, which is verified with all turning corners found in lazy-searches, to prevent repeated searches and allow Algorithm 5 to terminate. Removing the shrinking of free-sector is required for lazy-searches in R2 to find turning points, as R2 is built upon Algorithm 5.

Theorem 1. *For a set $\mathbf{L}_{\text{open}}$ returned by* SUCCESSORS_BASIC *in Algorithm 5, corners that yield the shortest path to $\mathbf{z}_t$ from $\mathbf{z}_s$ must be contained in $\mathbf{L}_{\text{open}}$.*

Proof. Fig. 11 provides the flow of Algorithm 5 and aids the proof.

If a turning corner $\mathbf{z}_\gamma$ satisfying condition (i) in Lemma 1.1 is found, all previously found corners along the same trace are

Algorithm 5 RayScan with source-pledge and simplified sector checks

```
1: function SUCCESSORS_BASIC(z_s, z_t, Λ_s = (Λ_L, Λ_R))
2:     (L_open, H) ← (∅, ∅)
3:     if z_t is in Λ_s then                          ▷ Is in sector
4:         Cast from z_s to z_t,
5:         Add any turn-points to L_open that the cast finds
6:         if cast collides at z_c then
7:             SCAN_BASIC(L, z_c, L_open)
8:             SCAN_BASIC(R, z_c, L_open)
9:         end if
10:    else
11:        Cast along Λ_L from z_s
12:        Add any turn-points found in cast to L_open
13:        if cast collides at z_L then
14:            SCAN_BASIC(R, z_L, L_open)
15:        end if
16:        Cast along Λ_R from z_s
17:        Add any turn-points found in cast to L_open
18:        if cast collides at z_R then
19:            SCAN_BASIC(L, z_R, L_open)
20:        end if
21:    end if
22:    return L_open
23: end function
24: function SCAN_BASIC(d, z_0, L_open)
25:    z_γ ← ∅
26:    Begin d-trace with source-pledge from z_0
27:    for each corner z_m found by trace do
28:        if trace goes out-of-map or no longer in Λ then
29:            return
30:        else if (d = L) ∧ (θ_{p,m} > 0) or
31:                (d = R) ∧ (θ_{p,m} < 0) then
32:            z_γ ← z_m
33:            break
34:        end if
35:    end for
36:    if z_γ ≠ ∅ and z_γ ∉ H then
37:        Push z_γ into H
38:        Cast from z_s to z_γ
39:        Add any turn-points to L_open that the cast finds
40:        if cast collides at z_c then
41:            SCAN_BASIC(L, z_c, L_open)
42:            SCAN_BASIC(R, z_c, L_open)
43:        else                                       ▷ Reaches z_γ
44:            Push z_γ into L_open
45:            Continue casting in same direction from z_γ
46:            Add
47:            if cast collides at z_b then
48:                SCAN_BASIC(d, z_b, L_open)
49:            end if
50:        end if
51:    end if
52: end function
```

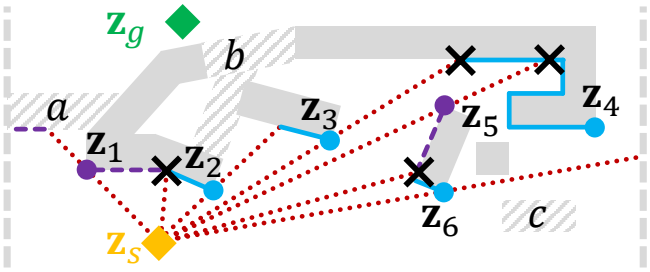

Fig. 11. Algorithm 5 finds corners $\mathbf{z}_1$ first, then $\mathbf{z}_2, \cdots, \mathbf{z}_6$.

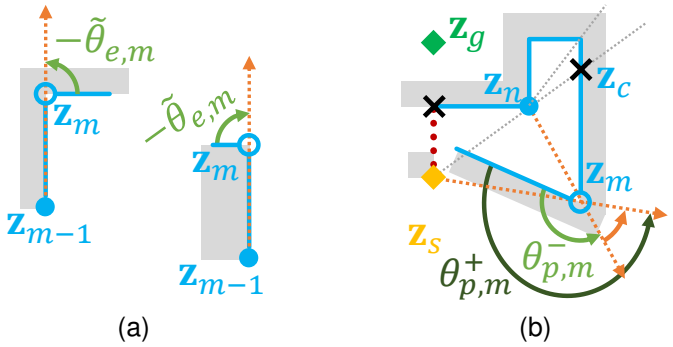

Fig. 12. Source-pledge adjustments in (a) Lemmas 2.1 and (b) 2.2

not verified for LOS due to Lemma 1.3 (line 32 of Algorithm 5). $\mathbf{z}_\gamma$ corresponds to, $\mathbf{z}_1$ to $\mathbf{z}_6$ in Fig. 11.

The algorithm tries to cast toward $\mathbf{z}_\gamma$. If $\mathbf{z}_\gamma$ is reached, $\mathbf{z}_\gamma$ is added to $\mathbf{L}_{\text{open}}$, and the cast continues in the same direction from $\mathbf{z}_\gamma$. When the cast collides (line 47 of Algorithm 5), another trace (SCAN_BASIC) begins on the same side. The trace can find additional turning corners satisfying condition (i) like $\mathbf{z}_3$ and $\mathbf{z}_4$. These corners can satisfy condition (iii) from the initial cast if the contours are contiguous, for example $\mathbf{z}_4$, when obstacle a does not exist. The corners are in an angular direction (AW or CW) that is further away from previous turning corners found from the initial cast. The cast occurs again for these turning corners in the invoked SCAN_BASIC (line 38 of Algorithm 5), repeating the recursions until one cast goes out-of-map, like $\mathbf{z}_6$.

Let the final cast occur on $\mathbf{z}_{\gamma,f}$, in the direction $\overrightarrow{\mathbf{z}_s\mathbf{z}_{\gamma,f}}$. If the edges traced from the initial cast to $\mathbf{z}_{\gamma,f}$ are contiguous, the shortest path must intersect $\mathbf{z}_{\gamma,f}$ to reach $\mathbf{z}_t$. The path cannot pass through undiscovered turning corners, like on obstacle c, as the path will be longer.

When the cast from $\mathbf{z}_s$ to $\mathbf{z}_\gamma$ collides, L and R scans are invoked on contours that are closer than previous casts (lines 41 and 42 of Algorithm 5). The turning corners $\mathbf{z}_5$ and $\mathbf{z}_6$ in Fig. 11 are found by the closer scans.

The algorithm continues until the closest turning corners are found that have LOS from $\mathbf{z}_s$. At least one of the turning corners must lie on the shortest path between $\mathbf{z}_s$ and $\mathbf{z}_t$. The visible turning corners are added to $\mathbf{L}_{\text{open}}$ and returned by SUCCESSORS_BASIC. □

Using the source-pledge, Algorithm 5 identifies less successors than RayScan. Successors are turning corners with LOS from $\mathbf{z}_s$. Unlike RayScan, all successors identified by Algorithm 5 are correct for non-convex obstacles.

IV. Correctness of R2

Algorithm 5 returns successors that lie on jagged edges caused by discretised slanted lines. The jagged edges are smoothed by pre-processing RayScan, except for larger jagged structures. Unlike RayScan, jagged structures and edges are bypassed in R2 by incorporating lazy-searches into Algorithm 5.

In Algorithm 5 and RayScan, a scan traces until one turning corner and returns from the trace. In R2, a scan begins with a lazy-search, which optimistically traces and casts to a target $\mathbf{z}_t$, primarily until two consecutive turning corners are found, allowing R2 to bypass jagged structures. Optimistic traces can continue after one turning corner is found, or go out-of-sector of the turning corner, before the lazy-search returns.

To find a consecutive turning corner, which lies in the free-sector of the first turning corner, the source-pledge along a trace that immediately follows the first must be **reset**:

Lemma 2.1. *If $\mathbf{z}_{m-1}$ is a turning corner, then the pledge is reset with $\theta_{p,m} = -\tilde{\theta}_{e,m}$ at $\mathbf{z}_m$.*

Proof. $\mathbf{z}_{m-1}$ becomes the new origin which the source-pledge uses to find turning points. The optimistic trace is equivalent to casting from $\mathbf{z}_{m-1}$ to $\mathbf{z}_m$, where Eq. 12 yields $-\tilde{\theta}_{e,m}$. □

The free-sector of the source $\mathbf{z}_s$ can be revisited by a lazy-search's optimistic trace, after tracing out-of-sector (not in the occupied-sector) of a previously discovered turning corner. To identify turning corners, the origin of the source-pledge must be readjusted to $\mathbf{z}_s$:

Lemma 2.2. *$\mathbf{z}_n$, a turning corner with respect to $\mathbf{z}_s$, is found by a lazy-search. The lazy-search traces and finds $\mathbf{z}_m$, which is out-of-sector of $\mathbf{z}_n$ with respect to $\mathbf{z}_s$ and not in the occupied-sector of $\mathbf{z}_n$.*

$$\tilde{\theta}^-_{s,m} = \left[\!\left[\text{atan2}\left(\overrightarrow{\mathbf{z}_n\mathbf{z}_m}\right) - \text{atan2}\left(\overrightarrow{\mathbf{z}_n\mathbf{z}_{m-1}}\right)\right]\!\right] \tag{28}$$

$$\tilde{\theta}^+_{s,m} = \left[\!\left[\text{atan2}\left(\overrightarrow{\mathbf{z}_s\mathbf{z}_m}\right) - \text{atan2}\left(\overrightarrow{\mathbf{z}_n\mathbf{z}_m}\right)\right]\!\right] \tag{29}$$

$$\theta_{p,m} = \tilde{\theta}^+_{s,m} + \tilde{\theta}^-_{s,m} - \tilde{\theta}_{e,m} + \tilde{\theta}_{p,m-1} \tag{30}$$

Proof. Before reaching $\mathbf{z}_m$, only exterior and interior edges with respect to $\mathbf{z}_n$ are traced, as $\mathbf{z}_m$ is a turning corner satisfying condition (i) in Lemma 1.3. Consider a topological curve of exterior edges with respect to $\mathbf{z}_n$, and an angle subtended by the curve at $\mathbf{z}_n$. The curve begins after an optimistic cast's collision point or after the source-pledge resets at $\mathbf{z}_n$, and is traced by an optimistic trace.

All interior edges immediately following the curve lie within the angular range subtended by the curve. The optimistic trace reaches its maximum angular displacement at the end of the curve when seen from $\mathbf{z}_n$. From Lemma 1.1, the trace moves in one angular direction (AW or CW) on exterior edges. For the trace to go out-of-sector of $\mathbf{z}_n$ at $\mathbf{z}_m$, $\mathbf{z}_m$ must lie immediately after an exterior edge $\mathfrak{e}_m$ with respect to $\mathbf{z}_n$.

Let $\mathbf{z}_c$ be the intersection of the line $\mathbf{z}_s\mathbf{z}_n$ with $\mathfrak{e}_m$, as shown in Fig. 12b. The line lies on the radius of the free-sector of $\mathbf{z}_n$ with respect to $\mathbf{z}_s$. If there are no obstacles between $\mathbf{z}_c$ and $\mathbf{z}_s$, $\mathbf{z}_c$ is the collision of a cast from $\mathbf{z}_s$ along the line. Therefore, $\mathfrak{e}_m$ is an exterior edge with respect to $\mathbf{z}_s$.

$\mathfrak{e}_m$ is a straight exterior edge with respect to both origins $\mathbf{z}_s$ and $\mathbf{z}_n$. The source-pledge $\theta_{p,m-1}$ lies in the same half (Q1/Q2 or Q3/Q4) for both origins and are at most π radians different and related by Eq. 29. □

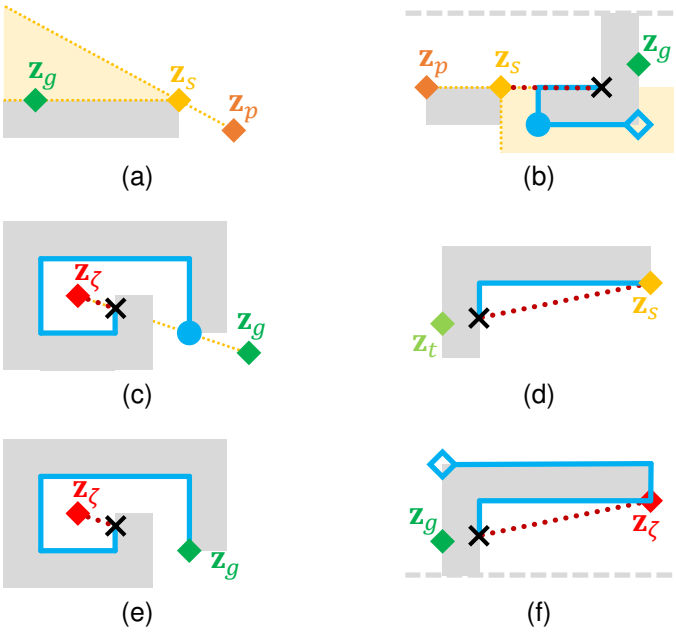

Fig. 13. (a,b) The free-sector includes both radii as $\mathbf{z}_g$ can lie on the radii, and traces cannot be terminated if their corners lie on the radii. (c) Due to radii inclusion, any trace finding a turning corner on the radii must be terminated. (d) Traces can be terminated if they revisit $\mathbf{z}_s \neq \mathbf{z}_\zeta$, or (e) reach $\mathbf{z}_t$. (f) $\mathbf{z}_s = \mathbf{z}_\zeta$ lies an infinitesimal distance away from the contour, allowing re-visits and R2 to be complete.

Lemma 2.3. *The lazy-search is terminable and returns successor candidates in a candidate stack* $\mathbf{\Gamma}$*. The candidates lie along a contiguous contour in a CW or AW order when seen from* $\mathbf{z}_s$*.*

Proof. In a lazy-search, all candidates in $\mathbf{\Gamma}$ are identified by Corollary 1.2 *and are turning corners*. When traces identify candidates or go out-of-sector of a candidate, Lemmas 2.1 and 2.2 readjusts the source-pledge.

The source-pledge identifies candidates if the lazy-search terminate properly. The lazy-search terminates when all TRACER functions terminate. The termination conditions, in Algorithm 4, are:

1) Line 6: The trace goes out-of-map.
2) Line 12: Trace is occluded by a parent candidate $\mathbf{z}_{p,\gamma}$.
3) Line 14: Re-discovered $\mathbf{z}_{p,\gamma}$.
4) Line 19: Re-discovered $\mathbf{z}_t$ or $\mathbf{z}_s$.
5) Line 22: Enters an occupied-sector of the origin $\mathbf{z}_o$,
6) Line 25: out-of-sector of source $\mathbf{z}_s$.
7) Line 34: Two consecutive turning corners are found.
8) Line 37: Finds a candidate on source's free-sector's radii.
9) Line 39: Finds a candidate that exists in $\mathbf{H}$.

Condition (1) occurs because traces that go out-of-map will not find candidates. For condition (2), any trace that becomes occluded by a parent candidate will not find visible candidates, like in Fig. 2b. For condition (3), when the lazy-search re-traces a previous trace from an ancestor scan and rediscovers a parent candidate $\mathbf{z}_{p,\gamma}$, the search repeats.

For condition (4), when a minor trace traced back to $\mathbf{z}_s$, the trace after $\mathbf{z}_s$ is repeated. When $\mathbf{z}_t$ is encountered, then the trace is occluded because SUCCESSORS initially failed to cast to it.

For condition (5), $\mathbf{z}_s \neq \mathbf{z}_\zeta$, and the origin $\mathbf{z}_o$ is either $\mathbf{z}_s$ or a prior candidate found by the lazy-search. When TRACER enters an occupied-sector, any turning corner found is occluded from $\mathbf{z}_s$. The occluded turning corners can only be reached by a candidate that has LOS from $\mathbf{z}_s$. The candidate is found by other SCANs or infinite-casts in SUCCESSOR.

For condition (6), optimistic traces find turning corners $\mathbf{z}$ that lie out-of-sector of $\mathbf{z}_s$ will cause the path $\mathbf{z}_p\mathbf{z}_s\mathbf{z}$ to be longer than $\mathbf{z}_p\mathbf{z}$, and not be searched.

For condition (7), the second turning corner lies in the free-sector of the first, causing subsequent traces to be occluded from the source $\mathbf{z}_s$. If the trace exits the free-sector and is visible, it will be re-discovered by another SCAN and lazy-search, following a cast to the first turning corner, which is a candidate.

Condition (8) states that a trace at $\mathbf{z}_m$ goes out-of-sector, if $\mathbf{z}_m$ satisfies condition (i) from Lemma 1.2 and lies on the source's free-sector's radii. Otherwise, after a lazy-search follows contours for a full circle around $\mathbf{z}_s = \mathbf{z}_\zeta$, an optimistic CASTER in the lazy-search can occur on $\mathbf{z}$, repeating the lazy-search after CASTER collides. SUCCESSORS will discover $\mathbf{z}_m$ during casts from $\mathbf{z}_s$ as well, allowing $\mathbf{z}_m$ to be ignored. The trace can proceed if $\mathbf{z}_m$ lies on the radii but does not satisfy condition (i), like in Fig. 13b, to allow the lazy-search to find candidates later.

R2 does not shrink free-sectors in recursive calls to SCAN, allowing lazy-searches to find correct turning points. Not shrinking free-sectors leads to repeated lazy-searches that rediscover the same turning corners as ancestor scans. By storing the turning corners into $\mathbf{H}$, repeated searches can end as soon as traces re-encounter the turning corners in $\mathbf{H}$, allowing R2 to terminate. Condition (9) stores only turning corners that are cast from $\mathbf{z}_s$, allowing faster iteration of $\mathbf{H}$ at every turning corner discovered.

Conditions (1), (3), (5), (7) and (8) allow minor traces to terminate lazy-searches when turning points are found in the free-sector of the most recent candidate, or if the lazy-search does not follow a contiguous contour. The terminating conditions allow only major traces, which are of the same sidedness as the SCAN, to find candidates, causing candidates to be in increasing or decreasing angular displacement from the cast that invoked the lazy-search's SCAN, as seen from $\mathbf{z}_s$. □

Lemma 2.4. SCAN *correctly identifies successors from* $\mathbf{\Gamma}$ *and is terminable.*

Proof. After the lazy-search, SCAN iterates over the candidate stack $\mathbf{\Gamma}$, starting from the candidate that is furthest from the SCAN's invoking cast. From Lemma 2.3, a contiguous contour is followed by the lazy-search and the stack is sorted in an angular order. When a candidate has LOS from $\mathbf{z}_s$, all candidates remaining in the stack can be discarded (line 8 in Algorithm 1), as shown in Fig. 2c. Otherwise, they are checked when invoked child SCANs return.

SCAN is identical to SCAN_BASIC in Algorithm 5 except for the former's lazy-searches replacing the latter's initial trace. Theorem 1, SCAN is complete and terminable, as the lazy-searches return correct successors from Lemma 2.3 and are terminable. □

Theorem 2. *R2 is complete, terminable and optimal as* SUCCESSORS *finds all relevant successors for a source* $\mathbf{n}_s$.

Proof. SUCCESSORS has an identical structure with SUCESSORS_BASIC in Algorithm 5. From Theorem 1 and Lemma 2.4, SUCCESSORS is complete and terminable, as the child SCANs are complete and terminable.

R2 is complete and terminable as SUCCESSORS is complete and terminable. SUCCESSORS is invoked for every node enqueued in the open-list $\mathbf{L}_{\text{open}}$, which finds successors to the nodes and enqueues them into $\mathbf{L}_{\text{open}}$.

R2 is optimal. Nodes enqueued into $\mathbf{L}_{\text{open}}$ are successors that lie in free-sectors of the nodes' sources, forming taut path segments with the latter's sources. The nodes are sorted within $\mathbf{L}_{\text{open}}$ with heuristic costs used in A*, which underestimates the shortest path cost. From Theorem 1, successors that lie on the shortest path are guaranteed to be found if the shortest path passes through the source. R2 is optimal as nodes are admissible, the $\mathbf{L}_{\text{open}}$ is sorted, and the shortest path lies on successors that are enqueued into $\mathbf{L}_{\text{open}}$. □

V. METHODOLOGY

R2 is programmed in C++17 and available at [16]. R2 is compared to the C++ Anya implementation from [17]. Both implementations are compiled with the `O3` optimisation flag, and are run on Ubuntu 20.04 LTS on Windows Subsystem Linux 2 and on one core of Intel i9-11900H at 4.9GHz.

R2 is tested on a wide variety of maps from [18] on binary occupancy grids, which are special cases of maps of polygons. The source-pledge is discretised to 8 directions [14], as traces can only occur along cardinal directions for binary occupancy grids, avoiding expensive $\text{atan2}(\cdot)$ calculations.

R2 and Anya implementations do not have diagonal blocking, allowing paths to pass through diagonally opposite occupied cells. The occupied cells are cardinally adjacent to free cells, like a 2×2 checkerboard. The passage through diagonally opposite occupied cells is ambiguous as the accurate positions of the obstacles are lost after map discretization, and can be impossible for the robot to pass through. The R2 implementation in [16] can be modified to allow diagonal blocking by setting `RSB_DIAG_BLOCK` to `1`.

TABLE V
SPEED-UPS OF R2 VS. ANYA

Map	Num. Cases	Pct. Faster	Mean SU	Med. SU
random512-10-0	1780	0.730	0.103	0.075
random512-40-3	3470	6.110	0.614	0.536
arena2	910	60.549	2.266	1.270
ht_mansion2b	1030	67.282	1.837	1.360
Denver_2_1024	3700	62.324	1.459	1.221
London_2_1024	3840	32.995	1.035	0.773
maze512-32-0	6170	94.084	2.373	2.536
maze512-1-0	12120	0.305	0.586	0.580

Num. Cases refer to the number of cases in the benchmark. *Pct. Faster* refers to the percentage of cases where R2 is faster. *Mean SU* refers to the mean speed-ups of R2 over Anya. For each case, the speed-up is calculated by dividing Anya's search times by R2's, regardless of path length. *Med. SU* refers to the median speed-up across all cases.

VI. RESULTS AND DISCUSSION

Selected results are shown in Table V and 14. Plots in 14 use R2's path lengths.

R2 can perform up to a hundred times faster than Anya if the start and goal have line-of-sight. The fast search time of such cases are noticeable as tails at the bottom left on row 2 of Fig 14, and tails at the top of row 3. The speed-ups are more evident when maps are larger, sparser and has fewer discontiguous contours, as R2 relies heavily on calculations on corners instead of free cells. When maps have exponentially more free-space cells than there are contours, like in Fig. 14a, 14b, 14f and 14g, then the longer the optimal paths, the larger the speed-ups. Such maps occur frequently in practice as smaller cells create smoother paths and the environmental representation is more accurate.

R2 does not perform well in maps with more discontinuous contours like in Fig 14h and jagged edges like in Fig 14d. Speed-ups may not be substantial if there are same number of free cells as there are contours, as shown in Fig. 14c.

Additional results are available in [16].

VII. CONCLUSION

R2 is a novel any-angle path planner which finds correct paths among polygonal non-convex obstacles. R2 can be run on binary occupancy grids, and is competitive to free-space expansion planners without pre-processing. R2 is competitive using three novel components: (a) lazy-searches that trace contiguous contours, (b) the source-pledge counter to identify successors in non-convex obstacles, and (c) successor candidate checking to reduce the number of candidates with line-of-sight.

R2 is fast on large sparse maps with little discontinuous contours, and these maps tend to occur in practice as fine-resolution maps are useful to create viable trajectories and better environment approximation. Free-space expansion planners tend to perform slowly on such maps. Results show that R2 can be about ten times faster than Anya on such maps, especially for queries with direct line-of-sight and are far apart.

REFERENCES

[1] P. E. Hart, N. J. Nilsson, and B. Raphael, "A formal basis for the heuristic determination of minimum cost paths," *IEEE Trans. on Syst. Sci. and Cybern.*, vol. 4, no. 2, pp. 100–107, July 1968.

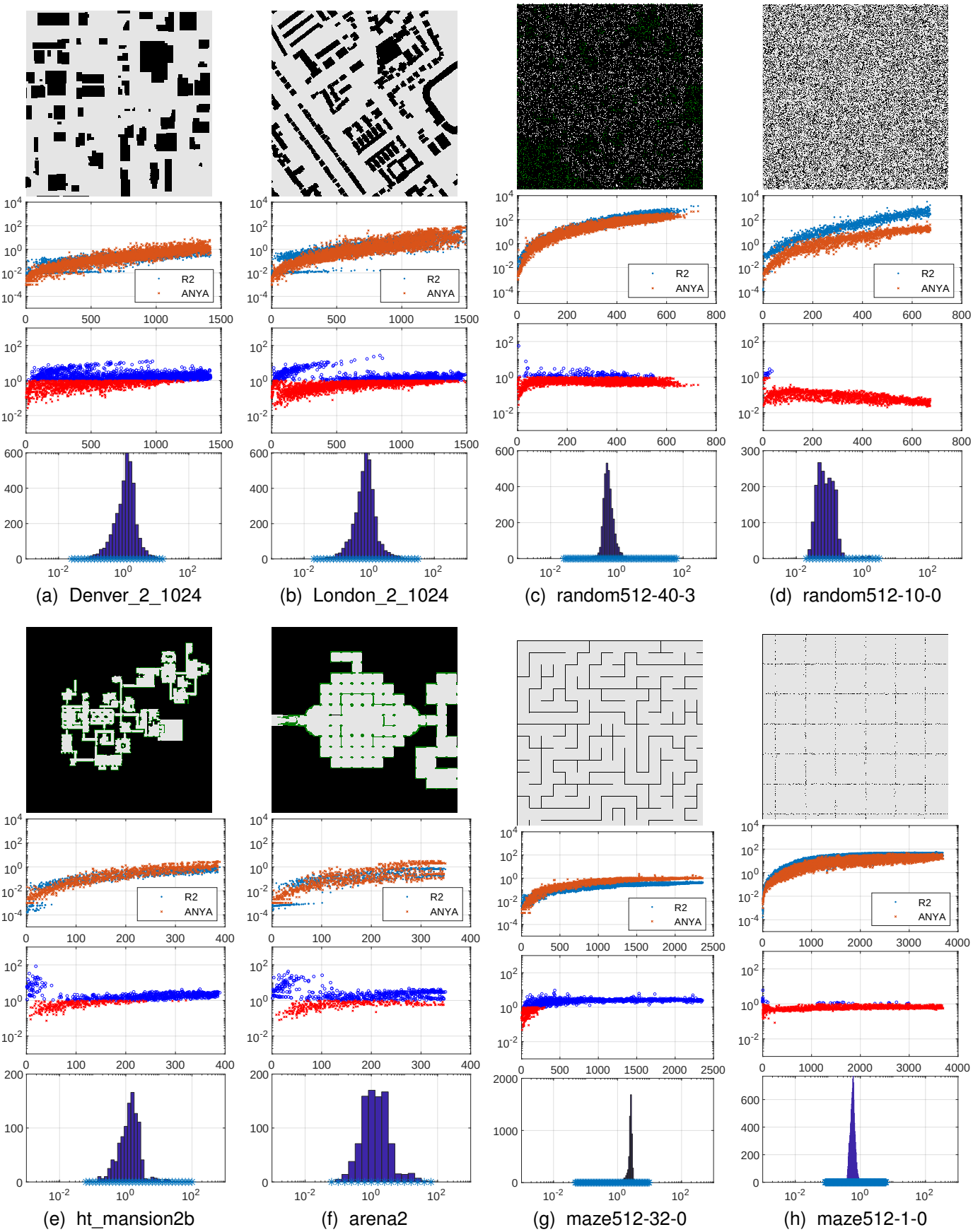

Fig. 14. R2 without diagonal blocking and Anya. Row 1: White pixels on map are accessible. Row 2: Solve time (ms) of R2 (blue) and Anya (orange) vs found path length in pixels. Row 3: Speed-ups of R2 vs. Anya by dividing Anya's solve time by R2's, vs found path length. Row 4: Histogram of speed-ups.

[2] E. W. Dijkstra *et al.*, "A note on two problems in connexion with graphs," *Numerische mathematik*, vol. 1, no. 1, pp. 269–271, 1959.

[3] K. Daniel, A. Nash, S. Koenig, and A. Felner, "Theta*: Any-angle path planning on grids," *J. of Artif. Intell. Res.*, vol. 39, pp. 533–579, 2010.

[4] A. Nash, S. Koenig, and C. Tovey, "Lazy theta*: Any-angle path planning and path length analysis in 3d," in *Proc. of the AAAI Conf. on Artif. Intell.*, vol. 24, no. 1, 2010.

[5] D. D. Harabor, A. Grastien, D. Öz, and V. Aksakalli, "Optimal any-angle pathfinding in practice," *J. of Artif. Intell. Res.*, vol. 56, pp. 89–118, 2016.

[6] R. Hechenberger, P. J. Stuckey, D. Harabor, P. Le Bodic, and M. A. Cheema, "Online computation of euclidean shortest paths in two dimensions," *Proc. of the Int. Conf. on Automated Planning and Scheduling*, vol. 30, no. 1, pp. 134–142, June 2020. [Online]. Available: https://ojs.aaai.org/index.php/ICAPS/article/view/6654

[7] K. Zhu and T. Zhang, "Deep reinforcement learning based mobile robot navigation: A review," *Tsinghua Science and Technology*, vol. 26, no. 5, pp. 674–691, 2021.

[8] L. Kavraki, P. Svestka, J.-C. Latombe, and M. Overmars, "Probabilistic roadmaps for path planning in high-dimensional configuration spaces," *IEEE Transactions on Robotics and Automation*, vol. 12, no. 4, pp. 566–580, 1996.

[9] S. Karaman, M. R. Walter, A. Perez, E. Frazzoli, and S. Teller, "Anytime motion planning using the rrt*," in *2011 IEEE International Conference on Robotics and Automation*, 2011, pp. 1478–1483.

[10] L. Gewali, S. Ntafos, and I. Tollis, "Path planning in the presence of vertical obstacles," *IEEE Transactions on Robotics and Automation*, vol. 6, no. 3, pp. 331–341, 1990.

[11] V. J. Lumelsky and A. A. Stepanov, "Path-planning strategies for a point mobile automaton moving amidst unknown obstacles of arbitrary shape," *Algorithmica*, vol. 2, no. 1, pp. 403–430, 1987.

[12] I. Kamon, E. Rimon, and E. Rivlin, "Tangentbug: A range-sensor-based navigation algorithm," *The Int. J. of Robot. Res.*, vol. 17, no. 9, pp. 934–953, 1998.

[13] H. Abelson and A. DiSessa, *Turtle Geometry: The Computer as a Medium for Exploring Mathematics*. Cambridge, MA: MIT Press, 1981.

[14] Y. K. Lai, P. Vadakkepat, A. Al Mamun, C. Xiang, and T. H. Lee, "Development and analysis of an improved prototype within a class of bug-based heuristic path planners," in *2021 IEEE 30th International Symposium on Industrial Electronics (ISIE)*. IEEE, 2021, pp. 1–6.

[15] P. Oprea, "A novel online any-angle path planning algorithm," Ph.D. dissertation, Univ. of Kent, Kent, 2017. [Online]. Available: https://kar.kent.ac.uk/71757/

[16] Y. K. Lai, "R2 github repository," 2022. [Online]. Available: \url{https://github.com/LaiYanKai/R2}

[17] T. Uras and S. Koenig, "An empirical comparison of any-angle path-planning algorithms," in *Eighth Annu. Symp. on Combinatorial Search*, 2015. [Online]. Available: http://idm-lab.org/anyangle

[18] N. Sturtevant, "Benchmarks for grid-based pathfinding," *Trans. on Comput. Intell. and AI in Games*, vol. 4, no. 2, pp. 144 – 148, 2012. [Online]. Available: http://web.cs.du.edu/~sturtevant/papers/benchmarks.pdf

VIII. Biography Section

Yan Kai Lai received his B.Eng. degree in Electrical Engineering from National University of Singapore, Singapore, in 2019. He is currently working toward the Ph.D. degree in robotics path planning with the National University of Singapore. His research interests include path-planning and simultaneous localisation and mapping in mobile ground robots. He also interested in robotics education.

Prahlad Vadakkepat received the B.Eng. degree (First Class Hons.) in Electrical Engineering from the Calicut University, Kerala, India, in 1986, and the M.Tech. and Ph.D. degrees from the Indian Institute of Technology Madras, Chennai, India, in 1989 and 1996, respectively. Since 1999, he is with the National University of Singapore, Singapore, where he is an Associate Professor. He is the Founder Secretary of the Federation of International Robot-Soccer Association and served as FIRA General Secretary from 2000 to 2016. His current research interests include robotics, AI, humanoid robotics, and frugal innovation.

Prof. Vadakkepat was a recipient of several international prizes for his teams of humanoid robots and robot soccer. He was the Editor-in-Chief of the Springer Reference Book on Humanoid Robotics, and an Associate Editor of the International Journal of Humanoid Robotics.

Abdullah Al Mamun Abdullah Al Mamun received the Bachelor of Technology (Honours) degree from Indian Institute of Technology, Kharagpur, India in 1985, and the Ph.D. degree from National University of Singapore in 1997. He is an Associate Professor in the department of Electrical and Computer Engineering at the National University of Singapore (NUS), and the Associate Head (UG programme) in the department. Prior to joining the NUS as faculty member, he worked in Siemens (Bangladesh), Data Storage Institute (Singapore), and Maxtor Peripherals (Singapore). Dr. Mamun's research interests are in the areas of mechatronic systems, precision servomechanism, and mobile robots.

Cheng Xiang received the B.S. degree from Fudan University in 1991; M.S. degree from the Institute of Mechanics, Chinese Academy of Sciences in 1994; and M.S. and Ph.D. degrees in electrical engineering from Yale University in 1995 and 2000, respectively. He is an Associate Professor and the area director of Control, Intelligent Systems and Robotics in the Department of Electrical and Computer Engineering at the National University of Singapore. His research interests include artificial intelligence, intelligent control, and systems biology.

Tong Heng Lee received the B.A. degree with First Class Honours in the Engineering Tripos from Cambridge University, England, in 1980; the M.Engrg. degree from NUS in 1985; and the Ph.D. degree from Yale University in 1987. He is a Professor in the Department of Electrical and Computer Engineering at the National University of Singapore (NUS); and also a Professor in the NUS Graduate School, NUS NGS. He was a Past Vice-President (Research) of NUS.

Dr. Lee's research interests are in the areas of adaptive systems, knowledge-based control, intelligent mechatronics and computational intelligence. He currently holds Associate Editor appointments in the IEEE Transactions in Systems, Man and Cybernetics; Control Engineering Practice (an IFAC journal); and the International Journal of Systems Science (Taylor and Francis, London). In addition, he is a past Deputy Editor-in-Chief of IFAC Mechatronics journal.